BNi2 + TiH_2 复合钎料钎焊 C/C 复合材料与 GH99 镍基高温合金

田晓羽[1]， 亓钧雷[1]， 张丽霞[1]， 梁迎春[3]， 李宏伟[1]， 冯吉才[1,2]
(1. 哈尔滨工业大学 先进焊接与连接国家重点实验室，哈尔滨 150001;
2. 哈尔滨工业大学 山东省特种焊接技术重点实验室，威海 264209;
3. 哈尔滨工业大学 机电工程学院，哈尔滨 150001)

摘 要: 采用 BNi2 + TiH_2 复合粉末钎料成功实现 C/C 复合材料与 GH99 镍基高温合金的钎焊，对焊后接头界面组织及力学性能进行了分析. 结果表明，焊后接头典型界面结构为 C/C 复合材料/Cr_3C_2 + *M*C + Ni(s,s) /*M*C + Ni(s,s) /Ni_3Si + Ni(s,s) /Cr_3C_2 + *M*C + Ni(s,s) /GH99 高温合金. 钎料中加入 TiH_2，可促进 C/C 复合材料母材的溶解，并在钎缝中部形成 *M*C 碳化物颗粒. 随着 TiH_2 含量的增加，钎缝中部 *M*C 形态由细小弥散向大片状转变. 当 TiH_2 含量为 3% 时，接头室温及 800，1 000 ℃高温抗剪强度最高，分别可达 40，19 及 10 MPa，接头强度高于 BNi2 钎料钎焊接头强度，并可有效保证接头高温使用性能.

关键词: C/C 复合材料; GH99; BNi2 + TiH_2 钎料; 界面组织; 抗剪强度
中图分类号: TG 454 **文献标识码:** A **文章编号:** 0253 - 360X(2014)05 - 0035 - 04

0 序 言

C/C 复合材料具有密度低、模量高、比强度大、线膨胀系数低等众多优点. 特别是其高温性能极其优异，在 2 000 ℃以上的高温下仍能保持良好的热力学性能. 因此 C/C 作为一种理想的高温结构材料，在航空航天领域得到了极广泛的应用[1-4]. 但是 C/C 制备复杂，很难生产出外形结构复杂、体积较大的构件，解决这一问题的方法之一就是将其与金属材料连接起来作为复合构件使用. 目前关于 C/C 复合材料与金属连接的研究还比较少，被连接金属也主要涉及铜以及钛合金等[5-7]. 但是铜及钛合金的使用温度都较低，这就大大限制了 C/C 复合材料的适用范围.

GH99 镍基高温合金属于沉淀强化型高温合金，其可在 1 000 ℃可靠使用，是一种广泛应用于航空航天领域的高温材料[8-10]，采用 GH99 与 C/C 连接制备复合构件，可大大提高构件使用温度，使 C/C 的热力学性能得到更加充分的发挥.

收稿日期: 2013 - 12 - 26
基金项目: 国家自然科学基金面上资助项目(51105108，E050803)；中央高校基本科研业务费专项资金资助项目(HIT. NSRIF. 2010113，2010115)；哈尔滨市科技创新人才研究专项基金资助项目(2010RFLXG005)

为确保接头高温使用性能，文中采用 BNi2 + TiH_2 粉末钎料对 C/C 与 GH99 进行钎焊，分析钎料中 TiH_2 含量对接头界面组织及力学性能的影响规律，优化钎料成分.

1 试验方法

文中所使用的 C/C 为准三维材料，通过化学气相沉积后石墨化获得; 钎料采用 300 目 BNi2 粉末钎料及 300 目 TiH_2 粉末超声震荡混合制备，钎料中 TiH_2 含量为 1% ~ 8%(质量分数). 将 C/C 切割成 8 mm × 8 mm × 7 mm 试块，选取与穿刺纤维方向平行面为焊接面; 将 GH99 切割成 10 mm × 10 mm × 2.5 mm 及 30 mm × 10 mm × 2.5 mm 试块用于组织分析以及性能测试. 焊前用砂纸对金属待焊表面逐级打磨，并使用丙酮溶液对待焊母材进行超声清洗. 试验在 Centorr 6-1650-15T 真空热压炉内进行，炉内真空度优于 1.0×10^{-3} Pa. 钎焊温度为 1 170 ℃，保温时间为 60 min.

文中采用 S-4700 扫描电镜对焊后接头界面组织进行观察，并采用 TN-4700X 射线能谱仪结合 Tecnai G2 F30 透射电镜以及 D/max-rb 旋转阳极 X 射线衍射仪对接头界面产物进行分析; 使用 Istron-1186 及 Istron-5569 电子万能试验机对接头室温及

高温抗剪强度进行测试.

2 试验结果与讨论

2.1 典型界面组织分析

图 1 为钎焊温度 1 170 ℃,保温时间 60 min 时使用 3% TiH_2 钎料钎焊 C/C 与 GH99 获得接头的典型界面形貌. 可以得到,接头界面结合良好,无裂纹、孔洞等缺陷. 由图 1a 中可以看到,接头界面可分为 4 个反应区. 如图 1b 所示,I 区主要为靠近C/C表面生成的深灰色条块状 A 相以及 A 表面析出的直径约为 10 mm 的白色颗粒 B 相; II 区主要为细小弥散的白色颗粒 C 相弥散分布在基体 D 相上. 如图 1c所示,通过对 III 区局部放大可以观察到边缘模糊的 E 相分布 D 相上; 而 IV 中主要可以观察到大量深灰色颗粒化合物 F 相及少量白色颗粒 G 相. 为确定各反应产物成分,对图 1 各相进行了能谱分析,所得结果如表 1 所示.

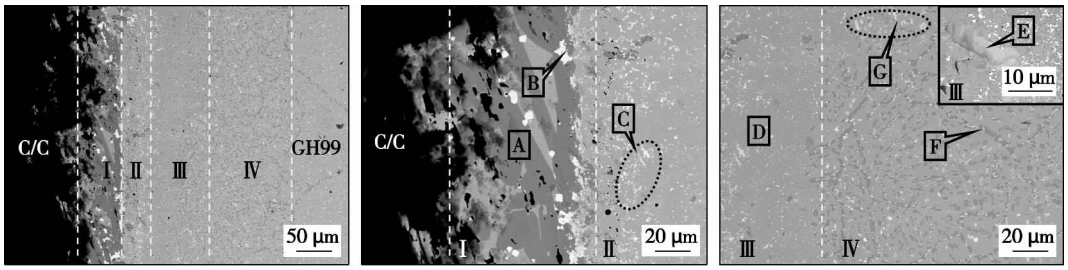

(a) 接头整体形貌 (b) C/C侧I区和II区形貌 (c) GH99侧III区和IV区形貌

图 1 1 170 ℃/60 min 条件下 3% TiH_2 钎料接头界面形貌

Fig. 1 Interfacial microstructure of the joint brazed with 3% TiH_2 braze alloy at 1 170 ℃ for 60 min

表 1 接头界面各相 EDS 成分分析结果(质量分数,%)

Table 1 EDS results of chemical compositions of each phase in weld interface

序号	Si	W	Mo	Ti	Cr	Ni	可能相
A	1.0	4.2	4.1	1.2	88.4	1.1	Cr_3C_2
B	3.2	18.3	19.7	42.2	10.9	5.7	*M*C
C	1.6	20.5	17.6	40.7	12.1	7.5	*M*C
D	7.0	4.0	1.3	1.1	3.7	82.9	Ni(s,s)
E	24.1	0.3	0.7	1.5	0.8	72.6	Ni_3Si
F	1.1	4.5	7.4	1.2	77.7	8.1	Cr_3C_2
G	2.2	20.9	15.3	44.7	9.2	7.7	*M*C

根据能谱结果推断,A 为铬的碳化物,由于Cr-C化合物种类众多且衍射峰较为接近,难于通过 XRD 辨别,因此对 A 相进行 TEM 分析,结果如图 2 所示,可确定 A 相为 Cr_3C_2. B 相主要含 Ti,Mo,W,Cr 及 C 元素,结合文献[11]及二元相图可得,上述各金属元素可在晶格中互相替换以构成复杂化合物,因此可推断 B 相为复杂金属碳化物 *M*C. C 相成分与 B 相相近,但体积更小,分布更为弥散,推断其仍为 *M*C 相,分析认为,当钎料熔化后,液态钎料中弥散分布的 Ti 与 C 结合作为 *M*C 形核质点,并随 GH99 溶解进入焊缝中的 Mo,W 等元素参与反应而长大,由于钎缝中 Ti,Mo,W 等元素含量有限因此 C 相体积较小. D 相主要含 Ni 元素,应为钎缝基体相 Ni(s,s). E 相应为 Ni-Si 化合物相,推断其为 Ni_3Si. F,G 相在靠近 GH99 母材侧生成,其中 F 与 A 成分相近,G 与 B 成分相近,且二者均呈细小的颗粒状,推断 F,G 仍为 Cr_3C_2 及 *M*C 相,由于该处液相中溶解的 Cr,Mo,W,Ti 等元素含量较高,因此在降温过程中上述过饱和元素将以颗粒状碳化物形式析出.

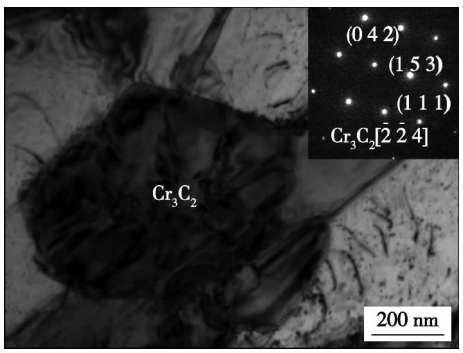

图 2 图 1 中 A 相 TEM 分析结果

Fig. 2 TEM results of phase A in Fig. 1

为进一步确定界面产物,对界面区进行 XRD 分析,结果如图 3 所示. 可以确定接头中有 Cr_3C_2, Ni_3Si 及 Ni(s,s) 生成,但由于 *M*C 相不具有固定的组成及晶体结构,缺乏 PDF 数据,因此还需进一步分析.

综合以上分析,BNi2 + TiH_2 接头典型界面结构可表示为C/C复合材料/Cr_3C_2(条块) + *M*C +

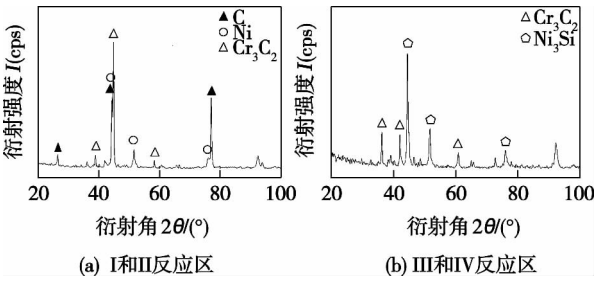

图 3　1 170 ℃/60 min 条件下 3% TiH_2 钎料接头界面 XRD 分析结果

Fig. 3　XRD results of joint brazed with 3% TiH_2 braze alloy at 1 170 ℃ for 60 min

Ni(s,s) /*M*C(弥散) + Ni(s,s) /Ni_3Si + Ni(s,s) /Cr_3C_2(颗粒) + *M*C(颗粒) + Ni(s,s) /GH99.

2.2　钎料中 TiH_2 含量对接头界面结构的影响

图 4 为 TiH_2 质量分数为 1%，5% 及 8% 钎料在 1 170 ℃，60 min 钎焊接头界面形貌. 使用 1% TiH_2 钎料时，由于钛含量较低，钛对界面影响较小，此时接头与 BNi2 钎料接头界面相似[12]，界面中部有块状 Cr_3C_2 及 *M*C 形成. 而当 TiH_2 含量增加，如图 1a 及图 4b 所示，C/C 侧 Cr_3C_2 生成量增加，界面中部主要生成大量细小弥散的 *M*C 及 TiC 颗粒. 由于 Ti 与 C 元素的亲和力较强，因此能促进 C/C 向钎缝中溶解，增加复合材料侧 Cr_3C_2 生成量. 此外溶解进入钎缝中的碳优先与液相中弥散分布的钛结合成为形核质点，液相中的 Mo，W 元素等在其基础上与 C 元素反应长大，最终以弥散的 *M*C 颗粒形式在钎缝中部析出. 弥散的 *M*C 颗粒可降低钎缝中部 Ni(s,s) 的弹性模量，从而降低 C/C 与钎缝的不匹配程度，

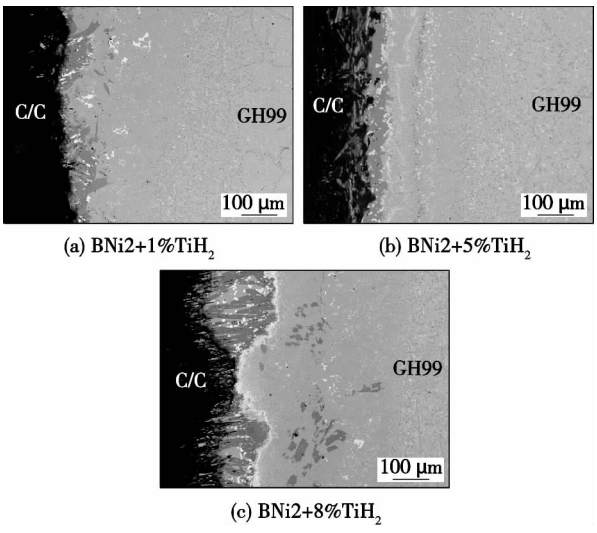

图 4　不同含量 TiH_2 钎料钎焊接头界面结构

Fig. 4　Interfacial microstructure of joints brazed using BNi2 + TiH_2 with different content of TiH_2 addition

缓解接头残余应力. 当 TiH_2 含量增至 8% 时，界面如图 4c 所示，此时钎缝中钛含量过高，C/C 溶解量进一步增加，复合材料侧形成大片状 Cr_3C_2 及 *M*C 层，钎缝中部除大量弥散的 *M*C 颗粒外，还有大量片状 TiC 出. 由于片状 TiC 的存在，钎缝塑性变形能力将被显著抑制，对接头力学性能造成不利影响.

2.3　钎料中 TiH_2 含量对接头力学性能的影响

图 5 为 1 170 ℃保温 60 min 时采用不同成分 BNi2 + TiH_2 钎料及 BNi2 钎料接头抗剪强度对比. 由图 5a 可知，随 TiH_2 含量增加，接头室温抗剪强度先升高后降低，当 TiH_2 含量为 3% 时，抗剪强度最高可达 40 MPa. 当 TiH_2 含量为 3% 和 5% 时，接头强度高于 BNi2 钎料接头强度. 由图 5b 可知，TiH_2 含量对接头 800 和 1 000 ℃高温抗剪强度影响规律与其对室温抗剪强度影响相似. 当 TiH_2 含量为 3% 时，800 和 1 000 ℃高温抗剪强度最高可达 19 和 10 MPa. 当 TiH_2 含量为 3 和 5% 时，接头抗剪强度高于 BNi2 钎料接头强度. 而目前国外对 C/C 与高温合金连接研究报道较少，仅有部分学者对 C/C 与铜的连接进行研究，结果表明 C/C 与铜接头抗剪强度不足 20 MPa[5,13].

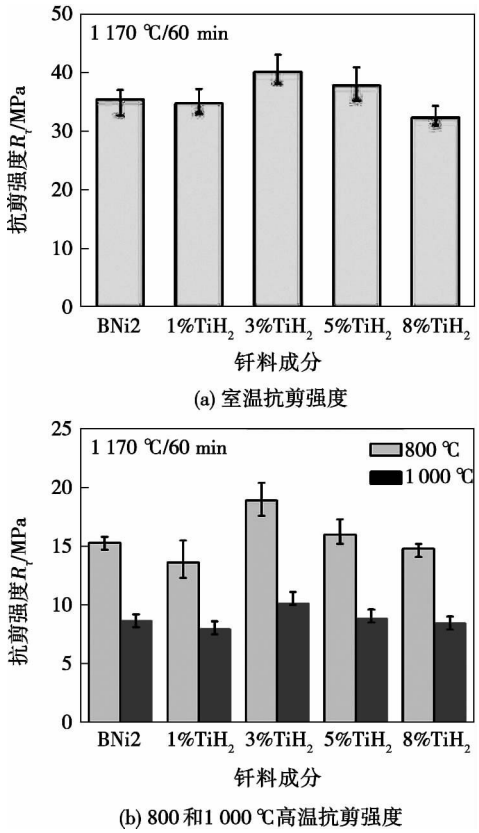

图 5　钎料 TiH_2 含量对接头抗剪强度的影响

Fig. 5　Effect of TiH_2 content in filler alloy on shear strength

结合前文 TiH_2 含量对界面影响的分析，当 TiH_2

含量较低时，界面与 BNi2 接头界面相近，仅在 C/C 侧 Cr_3C_2 层生成量略有增加，因此接头强度略有降低. 当 TiH_2 含量增加时，界面中部生成大量细小弥散的 *M*C 颗粒，从而有效降低钎缝中部组织弹性模量，缓解接头残余应力，提高接头抗剪强度. 当 TiH_2 含量进一步增加，钎缝中部形成的片状碳化物抑制钎缝组织塑性变形能力，从而恶化接头性能.

3 结 论

(1) 采用 BNi2 + TiH_2 复合粉末钎料成功实现 C/C 复合材料与 GH99 高温合金的钎焊，当钎焊温度为 1 170 ℃，保温时间为 60 min 时，采用 BNi2 + 3% TiH_2 钎料钎焊接头室温抗剪强度最高可达 40 MPa，800 和 1 000 ℃ 高温抗剪强度最高可达 19 和 10 MPa. 与 BNi2 钎焊接头相比强度有显著提高.

(2) 接头的界面结构从 C/C 至 GH99 侧可表示为：C/C 复合材料/Cr_3C_2(条块) + *M*C + Ni(s,s) / *M*C(弥散) + Ni(s,s) /Ni_3Si + Ni(s,s) /Cr_3C_2(颗粒) + *M*C(颗粒) + Ni(s,s) /GH99. 钎料中 TiH_2 含量增加，C/C 侧 Cr_3C_2 化合物层生成量增加，界面中部生成弥散 *M*C 颗粒，直至有大片状碳化物从钎缝中部析出.

参考文献：

[1] Fitzer E. The future of carbon-carbon composite [J]. Carbon, 1987, 25(2): 163 - 165.

[2] Lacoste M, Lacombe A, Joyez P. Carbon/carbon extendible nozzles [J]. Acta Astronaut, 2002, 50(6): 357 - 367.

[3] 秦优琼，冯吉才，张丽霞. C/C 复合材料与 TC4 钎焊接头的组织与断裂形式分析 [J]. 焊接学报，2007，28(3)：13 - 16.
Qin Youqiong, Feng Jicai, Zhang Lixia. Microstructure and fracture properties of carbon/carbon composite and TC4titanium alloy joint [J], Transactions of the China Welding Institution, 2007, 28(3): 13 - 16.

[4] Chen Junhua, Xu Guoxiang, Geng Haoran, *et al*. Study on vacuum brazing of C_f/C composites [J]. China Welding, 2007, 16(4): 56 - 59.

[5] Salvo M, Casalegno V, Rizzo S, *et al*. One-step brazing process to join CFC composites to copper and copper alloy [J]. Journal of Nuclear Materials, 2008, 374(1/2): 69 - 74.

[6] Cao Jian, Wang Houqin, Qi Junlei, *et al*. Combustion synthesis of TiAl intermetallics and their simultaneous joining to carbon/carbon composites [J]. Scripta Materialia, 2011, 65(3): 261 - 264.

[7] 黄 超，林铁松，何 鹏，等. TiBw/TC4 钛合金与 C/C 复合材料钎焊接头 [J]. 焊接学报，2011，32(7)：39 - 42.
Huang Chao, Lin Tiesong, He Peng, *et al*. Microsturcture of TiB_w/TC4 alloy and C/C composite brazed joint [J], Transactions of the China Welding Institution, 2011, 32(7): 39 - 42.

[8] 林铁松，何 鹏，韩 冷，等. GH99 合金液相扩散连接界面组织分析 [J]. 焊接学报，2012，33(3)：25 - 28.
Lin Tiesong, He Peng, Han Leng, *et al*. Microstructure analysis of TLP bonded joint of GH99 alloy [J]. Transactions of the China Welding Institution, 2012, 33(3): 25 - 28.

[9] 李海新，魏红梅，何 鹏，等. TiAl/Ti/Nb/GH99 扩散连接接头的界面组织结构及接头强度 [J]. 焊接学报，2012，33(9)：9 - 12.
Li Haixin, Wei Hongmei, He Peng, *et al*. Interfacial microstructure and bonding strength of diffusion bonded TiAl /Ti /Nb/GH99 alloy join [J]. Transactions of the China Welding Institution, 2012, 33(9): 9 - 12.

[10] Fan Chenglei, Yang Cunli, Liang Yingchun, *et al*. Optimality analysis of multiplex A-TIG welding flux for nickel base superalloy [J]. China Welding, 2007, 16(2): 46 - 50.

[11] Wang L, Xie L, Zhang L, *et al*. On the role of carbides during the recrystallization of a directionally solidified nickel-base superalloy [J]. Scripta Materialia, 2006, 55(5): 457 - 460.

[12] 田晓羽. C/C 复合材料 GH99 镍基高温合金钎焊工艺及机理研究 [D]. 哈尔滨：哈尔滨工业大学，2010.

[13] Casalegno V, Koppitz T, Pintsuk G, *et al*. Proposal for a modified non-active brazing alloy for joining CFC composites to copper [J]. Composite: Part B, 2014, 56: 882 - 888.

作者简介： 田晓羽，男，1985 年出生，博士研究生. 主要从事钎焊、新材料连接研究工作. Email: hittianxiaoyu@163.com

通讯作者： 张丽霞，女，副教授. Email: zhanglxia@hit.edu.cn

requirements of underwater wet welding for CCSE36 steel with the water depth of 30 m.

Key words: underwater wet welding; flux-cored wire; CCSE36 steel; mechanical property

Electric signals filtering of AC CMT welding based on wavelet analysis WANG Dianlong, ZHANG Zhiyang, LIANG Zhimin, WANG Jun (School of Materials Science and Engineering, Hebei University of Science and Technology, Shijiazhuang 050018, China). pp 17 – 20

Abstract: An improved threshold de-noise algorithm based on the general de-noise threshold algorithm was proposed. A processing function and an adjustment coefficient were added to fill the gap within the threshold range. It is aimed at achieving the flexibility to adjust the degree of attenuation and smoothing and improving the continuity of the reconstructed signal and the degree of approximation of signals. Coif wavelet was used to decompose the electrical signal of stainless steel welding by AC CMT for 3-tier, then the decomposed wavelet coefficients were processed by improved threshold de-noise algorithm. The results showed that by adjusting the adjustment coefficient flexibly, high-frequency noise can be removed well as the useful mutation component and the rule pulsation signals were held through the processing of improved algorithm. The attenuation of the useful signals was lower than that the soft threshold method performed and improved the approximation to the real signals. The improved threshold de-noise algorithm is suitable for filtering of electrical signals of AC CMT.

Key words: AC CMT; wavelet transformation; improved threshold method; filtering for signals

Finite element analysis on friction stir welding of aviation aluminum alloy plate WANG Hongfeng[1,2], WANG Jianli[1], ZUO Dunwen[2], SONG Weiwei[1], DUAN Xinglin[1,2] (1. School of Mechanical Electronic & Information Engineering, Huangshan University, Huangshan 245041, China; 2. College of Mechanical and Electrical Engineering, Nanjing University of Aeronautics and Astronautics, Nanjing 210016, China). pp 21 – 25

Abstract: According to characteristics of friction stir welding, the dynamic heat source model for characteristics of friction stir welding process has been established based on fully considering the friction generating heat between the each parts of the tool and the joining plate, and joining plate friction coefficient with the temperature changing law in the friction stir welding process. By which finite element simulation has been studied for friction stir welding of aviation aluminum alloy sheet. By comparison with simulation results and test results, it could be verified that the established dynamic heat source model and finite element analysis process are reasonable. The simulation results show that the friction stir welding residual tensile stress is concentrated in the joint region, the maximum residual tensile stress appears in the middle of the joint region, and the residual compressive stress appears at the both ends in the joint region and other areas.

Key words: friction stir welding; residual stress; aviation aluminum alloy; heat source model; FEM

Effect of Cr content on deposited metal toughness of weathering steel XIAO Xiaoming, PENG Yun, YANG Shuai, TIAN Zhiling (State Key Laboratory of Advanced Steel Processes and Products, Central Iron & Steel Research Institute, Beijing 100081, China). pp 26 – 30

Abstract: The effect of Cr content on microstructure and toughness in deposited metals of weathering steel were investigated by the tensile test, impact test, optical microscope (OM), transmission electron microscopy (TEM), scanning electron microscope (SEM) and electron back-scattered diffraction (EBSD), respectively. The results show that the microstructure consists of granular bainite, acicular ferrite and a few lath bainite for both deposited metals. Good impact toughness is obtained for both deposited metals. Comparing with 1.0% Cr containing deposited metal, the content of granular bainite increases while acicular ferrite decreases of 1.41% Cr containing deposited metal. And the yield strength, tensile strength have improved by 6%, 9%, respectively, but the impact toughness has dropped by 56%. The increasing of the content of M-A constituents and mean grain size, and the decreasing of the number of the large angle boundary of 1.41% Cr containing deposited metal, which cause the rising of the probability of the crack initiation and reducing the resistance to crack propagate, result in its worse toughness.

Key words: weathering steel; deposited metal; Cr content; microstructure; toughness

Effects of electron beam welding with filler wire process on surfacing weld appearance ZHAO Jian, ZHANG Binggang, LI Xiaopeng, FENG Jicai (State Key Laboratory of Advanced Welding and Joining, Harbin Institute of Technology, Harbin 150001, China). pp 31 – 34

Abstract: In this paper low carbon steel surfacing layers were formed on 304 stainless steel by electron beam welding with filler wire process to explain the relations between weld appearance and main process parameters. The effects of such welding parameters as electron beam, welding speed, wire feed rate, wire feeding angle and wire feed position on weld appearance were researched. The results showed that the match of weld heat input with wire feed rate was the main factor which determined weld appearance. In the same process, the width of the weld increased while the electron beam increased. Meanwhile, the depth of the weld increased with increasing of the wire feeding angle. In addition, the welding process could be more stable and precise when the front wire feed position was adopted.

Key words: surfacing; electron beam welding; filler wire; surface modification

Brazing of C/C composite and GH99 superalloy Using BNi2 + TiH_2 composite filler powder TIAN Xiaoyu[1], QI Junlei[1], ZHANG Lixia[1], LIANG Yingchun[3], LI Hongwei[1], FENG Jicai[1,2] (1. State Key Laboratory of Advanced Welding and Joining, Harbin Institute of Technology, Harbin 150001, China; 2. Shandong Provincial Laboratory of Special Welding Technology, Harbin Institute of Technology at Weihai, Weihai 264209, China; 3. School of Mechanical Engineering, Harbin Institute of Technology, Harbin 150001, China). pp 35 – 38

Abstract: The brazing of C/C composite and GH99 nickel base superalloy was successfully performed using BNi2 + TiH_2 brazing powder. The interfacial microstructure and mechanical properties of the brazed joints were investigated. The results show that, the typical microstructure of the joint is: C/C composite/Cr_3C_2 + MC + Ni(s,s) /MC + Ni(s,s) /Ni_3Si + Ni(s,s) /Cr_3C_2 + MC + Ni(s,s) /GH99. With the increasing of content of TiH_2, the dissolution of C/C substrate was enhanced, dispersed MC carbide particles formed in braze seam, and the modulus mismatch between C/C and filler alloy, the mechanical properties of the brazed joints were improved consequently. When using braze powder with 3% TiH_2 addition, the maximum shear strength of the brazed joints were obtained, which were 40 MPa at room temperature, 19 MPa at 800 ℃ and 10 MPa at 1 000 ℃. Comparing with brazed joints using BNi2 filler alloy, BNi2 + TiH_2 joints possess higher strength, and the high-temperature properties of the joints can be guaranteed.

Key words: C/C composite; GH99 superalloy; BNi2 + TiH_2 braze powder; interfacial microstructure; mechanical properties

Microstructure and mechanical properties of impact pressure transient liquid phase bonded Mg/Al LIU Meng´en[1,2], SHENG Guangmin[1] (1. College of Material Science and Engineering, Chongqing University, Chongqing 400044, China; 2. Chongqing Industry Polytechnic College, Faculty of Vehicle Engineering, Chongqing 401120, China). pp 39 – 42

Abstract: Diffusion bonding of magnesium alloy AZ31 and Al5083 was undertaken under an impact pressure in vacuum. The microstructural features, mechanical properties of the joints were investigated by scanning electron microscopy (SEM), energy Dispersive spectrometer(EDS), microhardness tester and x-ray diffractometer. The results show that the joints are formed four layers, such as magnesium alloy matrix, metallurgical reaction layer, diffusion layer and aluminum alloy matrix. There are the intermetallic compounds Mg_2Al_3, MgAl, $Al_{0.56}Mg_{0.44}$, and the highest hardness is 3 300 MPa in the joint zone. The tensile test results show that the tensile strength of the joint increases at first,then decreases, and an optimized bonding strength of up to 46MPa. The tensile fracture is mixture of quasi cleavage and dimple. There exists prevailing information asymmetry in the mg side and al side.

Key words: impact pressure; diffusion bonding; microstructure; tensile strength

Process characteristics of cold metal transfer spot welding for automotive dissimilar metals between magnesium and steel XU Qingwei[1], CAO Rui[1], CHEN Jianhong[1], WANG Peichung[2] (1. State Key Laboratory of Advanced processing and Recycling of Non-ferrous Metals, Lanzhou University of Technology, Lanzhou 730050, China; 2. GM R&D Center, Warren MI 48090, USA). pp 43 – 46

Abstract: The magnesium alloy AZ31B sheet and galvanized steel sheet were lapped by cold metal transfer spot welding. Using orthogonal test method to optimize process parameters and at the same time, by means of optical microscope, scanning electron microscopy and universal tensile testing machine, the microstructure and mechanical properties of welding joint were studied. The results show that satisfied weld appearance and properties can be obtained. The important sequence of process parameters are followed, size of hole on the galvanized steel sheet, wire feed speed, spot welding time. The joints are typical spot welding-brazing joint, which are composed by the brazing zone and the welding zone. The tensile shear load of joint can reach 3.12 kN, which is larger than that of Mg-Mg spot welding joints. The shear fracture and tear fracture dominate the fracture mode of the joint.

Key words: cold metal transfer spot welding; dissimilar metals; process characteristics; orthogonal test

Y-groove cracking test on the welding crack resistance of the NM400 steel WANG Lipeng, ZHOU Guangtao (College of mechanical engineering and automation, Huaqiao University, Xiamen 361021, China). pp 47 – 50

Abstract: Y-groove cracking test was conducted to study the welding crack resistance of NM400 steel. Assessment of welding crack resistance of steel NM400 consists of the surface crack rate, section crack rate and root crack rate, and the effects of preheating on the crack resistance of steel NM400 has been analyzed. Thermal elastic-plastic finite element method was applied to carry out a finite numerical simulation of welding process for samples used in Y-groove cracking test and transverse welding residual stress distribution and peak position were obtained. The results indicated that the root crack rate of the steel NM400 at room temperature reached a high value, and it could be decreased to zero when preheating at 150 ℃. Therefore, preheating before welding can improve the welding crack resistance of steel NM400. Otherwise, stress concentration occured at the root of the Y-groove. Local transverse residual stress which was larger than the yield strength of materials is mechanical factors causing cracks.

Key words: welding crack resistance; finite element simulation; preheating

Property of repair welding joint of A7N01 aluminium alloy YAN Zhongjie[1], CHEN Shuxiang[2], SHANG Zhe[3], LIU Xuesong[1], FANG Hongyuan[1] (1. State Key Laboratory of Advanced Welding and Joining, Harbin Institute of Technology, Harbin 150001, China; 2. CSR Sifang Locomotive and Rolling Stock. Co., LTD, Qingdao 26111, China; 3. Beijing Aerospace Xinfeng Mechanical Equipment. Co., LTD, Beijing 100070, China). pp 51 – 54

Abstract: The welding joint and repair welding joint of A7N01 aluminium alloy are analyzed in this paper, the mechanical properties of the welding joint before and after repair welding were studied by welding residual stress measurement, tensile test, micro-hardness test, metallographic observation and fracture toughness test, respectively. Based on the fracture toughness theory, the critical crack length of the structure before and after repair welding is calculated. With the initial crack length determined by metallographic observation, the residual fatigue life before and after repair welding is calculated using Paris for-